phys. stat. sol. (c) **3**, No. 6, 1854–1857 (2006) / **DOI** 10.1002/pssc.200565467

Anisotropy of the Γ-point effective mass and mobility in hexagonal InN

T. Hofmann[*1], **T. Chavdarov**[1], **V. Darakchieva** [2], **H. Lu** [3], **W. J. Schaff** [3], and **M. Schubert** [4]

[1] Institut für Experimentelle Physik II, Universität Leipzig, 04103 Leipzig, Germany
[2] Department of Physics and Measurement Technology, Linköping University, 581 83 Linköping, Sweden
[3] Department of Electrical and Computer Engineering, Cornell University, USA
[4] Department of Electrical Engineering and Center for Materials Research and Analysis (CMRA), University of Nebraska-Lincoln, Lincoln, USA

Received 24 October 2005, accepted 23 December 2005
Published online 17 May 2006

PACS 73.50.Dn, 78.20.Ls, 78.30.Fs, 78.66.Fd

We determine the anisotropic electron effective mass and mobility parameters in wurtzite InN thin films with free electron concentration N from 1.8×10^{17} cm^{-3} to 9.5×10^{18} cm^{-3} using Infrared Magneto-optic Generalized Ellipsometry. The room-temperature measurements were carried out with magnetic fields up to 4.5 T. For the Γ-point we estimate $m_{\perp}^{\star} = 0.047m_0$ and $m_{\parallel}^{\star} = 0.039m_0$ for polarization perpendicular and parallel to the c-axis, respectively. Scattering by impurities or ionized donors may explain the decrease of mobility for polarization parallel to the c-axis from 1600 cm^2/(Vs) to 800 cm^2/(Vs) with increase in N, where the perpendicular mobility is further decreased, likely caused by additional grain boundary scattering.

1 Introduction

InN receives continued attention due to its potential use in group-III nitride based optoelectronic devices [1]. Crucial for understanding of electrical and optical performance is the precise knowledge of intrinsic parameters such as the Γ-point conduction band curvature and the electron mobility, for example. The electron effective mass parameters has revealed substantial nonparabolicity upon renewed investigations, concordant with recent realization that the InN band gap is narrower than previously thought [2–5]. We present here a study of the anisotropy of electron effective mass and mobility in wurtzite InN employing a newly developed optical precision technique: Infrared Magneto-optic Generalized Ellipsometry (IRMOGE) proceeding beyond earlier achievements were we used combined Infrared Spectroscopic Ellipsometry (IRSE) and electrical Hall effect measurements for InN effective mass determination. (Reviews on similar matter are in Refs. [3, 6].) IRMOGE dispenses with electrical Hall effect measurements, which was demonstrated successfully for III-V compound layer structures [7, 8]. Specifically, we apply IRMOGE for the first time to a situation, where both mobility and effective mass parameters potentially differ for polarizations parallel or perpendicular to a certain direction, here the InN lattice c-axis.

2 Experimental

Unintentionally-doped n-type InN epilayers were grown by molecular beam epitaxy on GaN/AlN/c-plane sapphire (Tab. 1). Structural and electrical characterization were performed by X-ray analysis and Hall effect measurements. The IRSE setup was operated for determination of Mueller matrix elements M_{ij} as well as standard ellipsometry parameters Ψ, Δ [9]. IRMOGE data were obtained with the samples

* Corresponding author: e-mail: tino.hofmann@physik.uni-leipzig.de, Phone: +49 341 9732 694, Fax: +49 341 9732 699

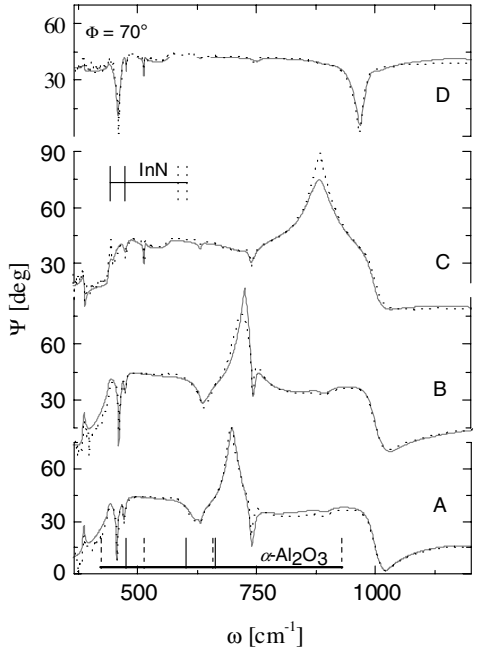

Fig. 1 InN/GaN/AlN/c-sapphire experimental (dotted) and best-model calculated (solid lines) IRSE Ψ spectra at $\mu_0 H = 0$. Labels A-D as in Tab. 1.

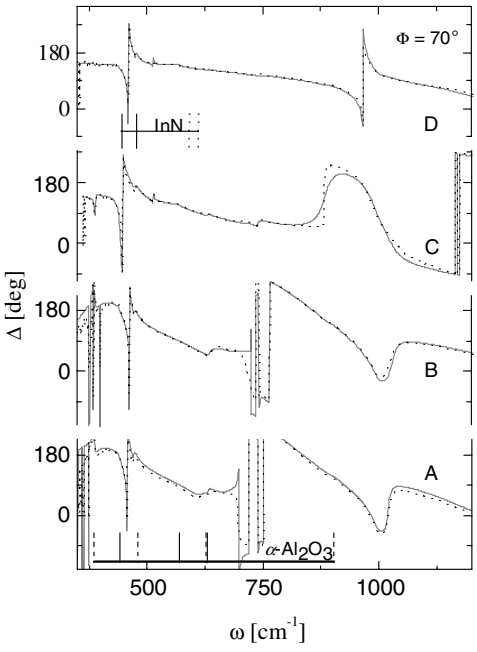

Fig. 2 Same as Fig. 1 for Δ. Brackets indicate reststrahlen bands of InN and sapphire, with solid vertical bars at the TO, and dashed vertical bars at the LO mode frequencies.

placed within a superconducting magnetocryostat (OXFORD) at 45° angle of incidence and magnetic field direction parallel to the incident radiation beam ("OMO" setup in Ref. [8]) in three steps: (i) with $\mu_0 H$=0, (ii) $\mu_0 H = +4.5$ T, and (iii) $\mu_0 H = -4.5$ T. Ψ, Δ data were obtained at 70° angle of incidence with samples outside the magnetocryostat. All data were combined within a model data analysis, where parameterized model functions and thickness parameters were varied to match all data sets simultaneously. The models required for best-match calculations were set as done and described in Refs. [3, 6–8, 10, 11], except for the InN-layer Drude contribution, which is now a tensor in the laboratory Cartesian coordinates (x,y,z) [12]:

$$\boldsymbol{\varepsilon}^{(\mathrm{FC\text{-}MO})}(\omega) = \frac{-1}{\omega} \begin{bmatrix} (\omega_\mathrm{p}^{*2})_\perp & 0 & 0 \\ 0 & (\omega_\mathrm{p}^{*2})_\perp & 0 \\ 0 & 0 & (\omega_\mathrm{p}^{*2})_\parallel \end{bmatrix} \left\{ \omega \boldsymbol{I} + i \begin{bmatrix} \gamma_{\mathrm{p},\perp} & 0 & 0 \\ 0 & \gamma_{\mathrm{p},\perp} & 0 \\ 0 & 0 & \gamma_{\mathrm{p},\parallel} \end{bmatrix} - i \begin{bmatrix} 0 & -h_3 & h_2 \\ h_3 & 0 & -h_1 \\ -h_2 & h_1 & 0 \end{bmatrix} \begin{bmatrix} \omega_{\mathrm{c},\perp} & 0 & 0 \\ 0 & \omega_{\mathrm{c},\perp} & 0 \\ 0 & 0 & \omega_{\mathrm{c},\parallel} \end{bmatrix} \right\}^{-1} .$$

Here we assign $\mu_0 \boldsymbol{H} = \mu_0 H(h_1, h_2, h_3)$ with H as the magnitude of $\boldsymbol{H}$, $(\omega_\mathrm{p}^{*2})_i = Ne^2/(\varepsilon_0 m_j^\star)$ is the unscreened plasma frequency, $\omega_{\mathrm{c},j} = q\mu_0 H/(m_j^\star)$ is the cyclotron frequency, and $\gamma_{\mathrm{p},i} = q/(\mu_i m_i^\star)$ is the plasmon broadening parameter for polarization i ="$\parallel$", "$\perp$" to the InN c-axis ($\boldsymbol{I}$ is the unit tensor, ε_0 and μ_0 are the vacuum permittivity and permeability, $q = -|e|$ is the elementary charge). Parameters electron density N, effective mass $m_i^\star$, and mobility μ_i were then calculated therefrom.

3 Results and discussion

Figures 1, 2 depict experimental and best-model calculated IRSE spectra from all samples listed in Tab. 1 at $\mu_0 H = 0$. From top to bottom, the InN layer electron density decreases (cf. Fig. 1 in Ref. [13]). The best-model analysis yields phonon mode frequencies and broadening parameters as discussed in Ref. [10], and specifically $\omega^2_{\mathrm{p},\perp}$, $\omega^2_{\mathrm{p},\parallel}$, and $\gamma_{\mathrm{p},\perp}$, $\gamma_{p,\parallel}$. Figs. 3 and 4 present IRMOGE spectra. The data are differences between Mueller matrix spectra measured at $\mu_0 H = +4.5$ T and those measured at $\mu_0 H = -4.5$ T. The best-model calculated and the experimental data are in excellent agreement. The model calculations for data points in Figs. 3 and 4 require only $\omega_{\mathrm{c},\perp}$ and $\omega_{\mathrm{c},\parallel}$ as additional parameters. All other model parameters are already defined by matching the spectra in the field free arrangement in Figs. 1, 2. Table 1 and Figs. 5, 6 contain our best-model parameters for N, $m^\star_i$, μ_i for polarization parallel and perpendicular to the InN c-axis. Fig. 5 summarizes previous data for $m^\star$, obtained from combined infrared spectroscopy and Hall effect analysis. The effective mass determined in Refs. [2, 5] must be related to polarization perpendicular c. Kasic *et al.* did not detect substantial anisotropy of the effective mass. This is concordant with our observation here, where substantial differences between $m^*_\parallel$ and $m^*_\perp$ was not observed for $N > 10^{19}\mathrm{cm}^{-3}$. Applying Kane's two-band **kp** model for both polarizations results in $m^\star_\perp$ = 0.047m_0 and $m^\star_\parallel$ = 0.039m_0 at the bottom of the conduction band. The electron mobility parameters decrease with increasing concentration linearly within the double-log presentation in Fig. 6, and which is expected if ionized-impurity or donor-site scattering dominates [11]. We find $\mu_\parallel > \mu_\perp$, likely due to additional scattering across grain boundaries.

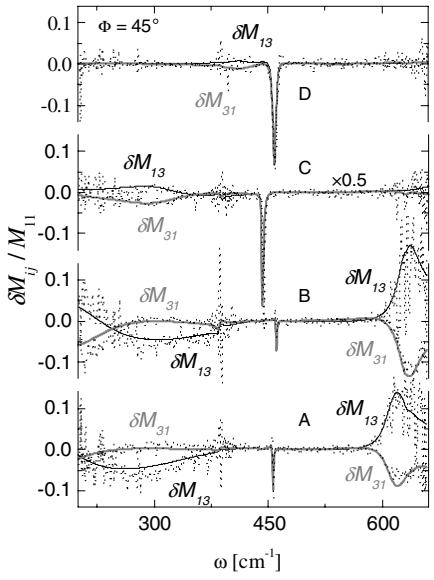

Fig. 3 Room-temperature experimental (dotted lines) and best-model (solid lines) Mueller matrix spectra M_{13}, M_{31} obtained by IRMOGE at Φ_a = 45°. The spectra are differences between those obtained at $\mu_0 H$ = -4.5 T and +4.5 T. Labels A-D as in Tab. 1.

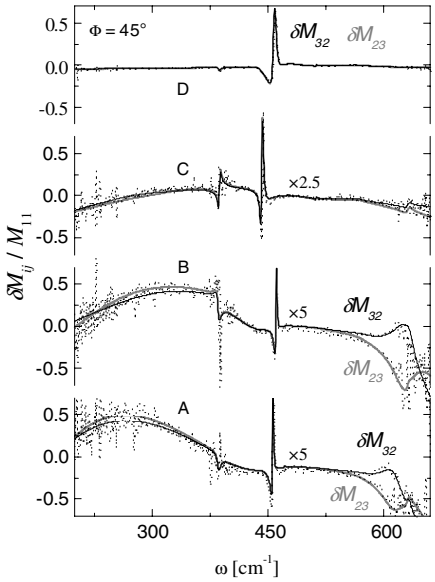

Fig. 4 Same as Fig. 3 for M_{23}, M_{32}. Spectra in Figs. 3 and 4 provide sufficient information to differentiate electron mobility and effective mass for polarization parallel and perpendicular to the InN c axis.

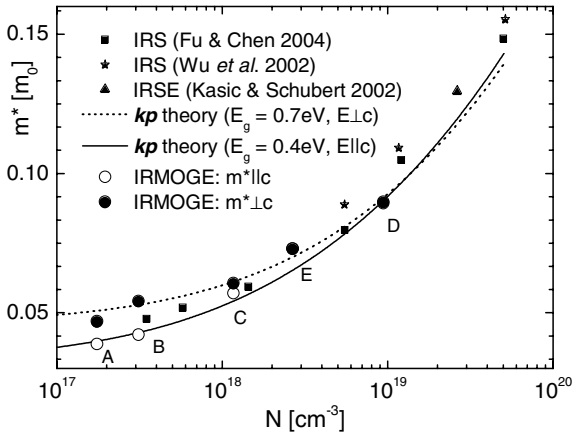

Fig. 5 Wurtzite InN effective mass parameters obtained in this work (IRMOGE), in comparison with previous reports from combined infrared spectroscopy and Hall-effect measurements and ***kp*** calculations.

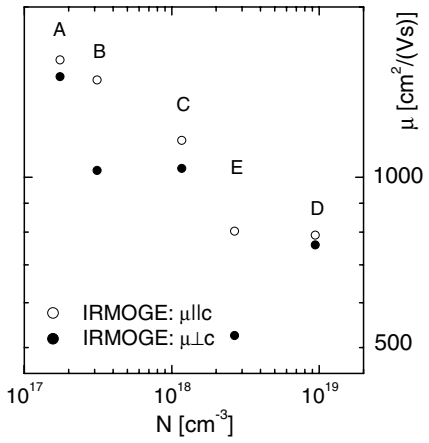

Fig. 6 Anisotropic optical electron mobility parameters obtained in this work.

4 Summary

In summary, we report on the anisotropic electron effective mass and mobility parameters in wurtzite InN thin films with free electron concentration N from 1.8×10^{17} cm^{-3} to 9.5 $\times10^{18}$ cm^{-3}.

Table 1 Best-model calculated sample parameters (layer thickness and free-charge-carrier parameters) obtained by simultaneous analysis of the IRSE and IRMOGE data.

Sample	d_{AlN} [nm]	d_{GaN} [nm]	d_{InN} [nm]	N [cm^{-3}]	$\mu_{\parallel}$ [cm^2/(Vs)]	$\mu_{\perp}$ [cm^2/(Vs)]	$m^*_{\parallel}$ [m_0]	$m^*_{\perp}$ [m_0]
A	26	396	1545	1.75×10^{17}	1613	1506	0.039	0.047
B	26	448	1356	3.12×10^{17}	1486	1028	0.042	0.054
C	52	128	645	1.17×10^{18}	1162	1037	0.057	0.060
D	10	222	540	9.41×10^{18}	790	759	0.090	0.090
E	244	-	519	2.7×10^{18}	803	525	0.073	0.073

Acknowledgements M.S. acknowledges support by the Deutsche Forschungsgemeinschaft grant SCHUH1338/3-1.

References

[1] H. Lu, W. J. Schaff, J. Hwang, H. Wu, G. Koley, and L. F. Eastman, Appl. Phys. Lett. **79**, 1489 (2001).
[2] S. P. Fu and Y. F. Chen, Appl. Phys. Lett. **85**, 1523 (2004).
[3] A. Kasic et al., phys. stat. sol. (c) **0**, 1750 (2003).
[4] I. Vurgaftman and J. R. Meyer, J. Appl. Phys. **94**, 3675 (2003).
[5] J. Wu et al., Phys. Rev. B **66**, 201403 (2002).
[6] M. Schubert, Infrared Ellipsometry on Semiconductor Layer Structures (Springer, Berlin, 2004).
[7] T. Hofmann, M. Schubert, C. M. Herzinger, and I. Pietzonka, Appl. Phys. Lett. **82**, 3463 (2003).
[8] M. Schubert, T. Hofmann, and C. M. Herzinger, J. Opt. Soc. Am. A **20**, 347 (2003).
[9] H. Thompkins and E. A. Irene (Eds.), Handbook of Ellipsometry (William Andrew Publishing, 2004).
[10] V. Darakchieva et al., Appl. Phys. Lett. **84**, 3636 (2004).
[11] P. Yu. and M. Cardona, Fundamentals of Semiconductors (Springer, New York, 1999).
[12] C. Pidgeon, in: Handbook on Semiconductors, edited by M. Balkanski (North-Holland, Amsterdam, 1980).
[13] A. Kasic, M. Schubert, S. Einfeldt, D. Hommel, and T. Tiwald, Phys. Rev. B **62**, 7365 (2000).